RSC Advances

PAPER

View Article Online
View Journal | View Issue



Cite this: *RSC Adv.*, 2024, **14**, 14425

# Preparation and application of stimuli-responsive PET TeMs: RAFT graft block copolymerisation of styrene and acrylic acid for the separation of water–oil emulsions

Indira B. Muslimova,[ab] Nurdaulet Zhumanazar,[b] Galina B. Melnikova,[ac] Arman B. Yeszhanov,[ab] Zhanna K. Zhatkanbayeva,[a] Sergei A. Chizhik,[c] Maxim V. Zdorovets,[ab] Olgun Güven[d] and Ilya V. Korolkov*[ab]

Stimuli-responsive membranes play an important role in the fields of biomedicine, food and chemical industries, and environmental applications, including separation of water–oil emulsions. In this study, we present a method to fabricate pH-sensitive membranes using UV-initiated RAFT graft copolymerization of styrene (ST) and acrylic acid (AA) on poly(ethylene terephthalate) (PET) track-etched membranes (TeMs). The optimization of polymerization conditions led to successful grafting of polystyrene (PS) and poly(acrylic acid) (PAA) onto PET TeMs, resulting in membranes with stable hydrophobicity and pH change responsiveness. The membranes show a contact angle of 65° in basic environments (pH 9) and 97° in acidic environments (pH 2). The membranes were characterized by atomic force microscopy (AFM), scanning electron microscopy with energy dispersive X-ray spectroscopy (SEM-EDX), thermogravimetric analyses (TGA), Fourier transform infrared spectroscopy (FTIR), contact angle (CA) methods. The PET TeMs-*g*-PS-*g*-PAA exhibited good performance in separating water–oil emulsions with a high efficiency of more than 90% and flux for direct chloroform–water 2500 L $m^{-2}$ $h^{-1}$ and reverse emulsions of benzene–water 1700 L $m^{-2}$ $h^{-1}$. This method of preparing stimuli-responsive membranes with controlled wettability and responsiveness to environmental pH provides versatility in their use in separating two types of emulsions: direct and reverse.

Received 20th March 2024
Accepted 25th April 2024

DOI: 10.1039/d4ra02117g

rsc.li/rsc-advances



## 1 Introduction

While the pivotal role of oil in sustaining the global economy is undeniable, it is equally imperative to address the environmental repercussions associated with its extraction, processing, and utilization. The versatility of oil extends across vital sectors such as heat, electricity, transportation, and the chemical industry, where it serves as the backbone for an array of essential products and processes, including fuels, motor oils, organic solvents, plastics, rubbers, varnishes, asphalt, and paraffin.

However, the unintended consequences of oil-related activities are becoming increasingly apparent. Oil spills, emissions from refineries, and anthropogenic impacts have given rise to the prevalence of water–oil emulsions in water systems.[1,2] This not only poses a significant threat to ecosystems but also jeopardizes human health, prompting the allocation of substantial financial resources for the remediation of water–oil emulsions.[3]

In light of these challenges, there is a pressing need for innovative and sustainable solutions to address the environmental impact of oil-related activities. Although various methods such as floatation,[4] coagulation,[5] and extraction[6] have been used for this purpose, there is currently a need for the development of advanced separation methods, which can be achieved *via* new types of membranes[7,8] and modification methods.[9–11]

One promising avenue is the application of membrane technology in the separation of emulsions,[2,12–14] which is also reflected in our previous works[3,15,16] using modified TeMs based on PET for the separation of water–oil emulsions. TeMs, due to a number of advantages (narrow pore size distribution and precise control of the number of pores per $cm^2$), are gaining interest in separation processes as model membranes.[17] Polycarbonate (PC), polypropylene (PP), poly(vinylidene fluoride)

[a]*L.N. Gumilyov Eurasian National University, Satpaev Str., 2, Astana 010000, Kazakhstan. E-mail: galachkax@gmail.com; arman_e7@mail.ru; mzdorovets@gmail.com; zhanna01011973@mail.ru*

[b]*The Institute of Nuclear Physics, Ibragimov str. 1, Almaty, 050032, Kazakhstan. E-mail: nurdauletzhumanazar@gmail.com; i.korolkov@inp.kz; Tel: +7-705-179-9083*

[c]*The National Academy of Sciences of Belarus, P. Brovki Str., 15, 220072 Minsk, Belarus. E-mail: chizhik@gmail.ru*

[d]*Hacettepe University, Beytepe, Ankara 06800, Turkey. E-mail: guven@hacettepe.edu.tr*

(PVDF), polyimides (PI), and PET are the most frequently used polymer substrates for TeMs. Among them, PET is thermally stable, chemically inert to acids and organic solvents, mechanically strong, and the etching technology does not require special and complicated procedures.[17,18] Our research group is one of the first to use modified PET TeMs to separate water–oil mixtures. There are known works using PET material as a matrix for the development of membranes, fabrics, and nanofibers for the separation of water–oil emulsions,[19–22] but there are only several works using PET TeMs for this purpose.[3,15,16] In this context and considering the successful application of PET TeMs in the separation of water–oil emulsions, we continued our work on the fabrication of innovative stimuli-responsive membranes by UV-initiated reversible addition–fragmentation chain transfer (RAFT) copolymerization.[3,15,16,23] RAFT polymerization allows to obtain firstly block copolymers and secondly prevents uncontrolled chain growth, *i.e.*, allows to synthesize polymers with a well-defined and narrow distribution of molecular weights, also called low polydispersity index.[24–28] Controlling the conversion and molecular weight of polymerization *via* the RAFT mechanism helps to prevent filling and blocking of narrow pores of PET TeMs.

Unlike traditional membranes, which typically have static (unchanging properties), stimuli-responsive polymers are materials that change their properties (wettability, permeability, porosity, phase transition, *etc.*) in response to external stimuli (changes in pH, temperature, ion concentration, light irradiation, electric field, and other factors).[29,30] These polymers can be designed to change the properties of the membrane surface, for example, controllable hydrophilicity, hydrophobicity, and pore sizes, in response to a change in stimuli. In this regard, stimuli-responsive materials find useful applications in various fields such as filtration, controlled drug delivery, sensing, and affecting their interaction with water and oil.[16,30–40]

pH-Responsive polymers are polymers containing acidic (carbonic, sulfonic acids, *etc.*) or basic (amines, pyridines, *etc.*) groups that give or take protons depending on pH.[16,30,41,42] Thus, acquiring pH-responsive polymers changes the conformation of the chain (stretching, straightening, self-assembly), which in turn leads to swelling or contraction of the polymer.[30,43] This phenomenon was the main idea of our previous work,[16] where polystyrene (PS) was grafted to the surface of PET TeMs by UV-initiated RAFT copolymerization to form a stable hydrophobic layer, followed by grafting a pH-responsive polymer, poly-4-vinylpyridine (P4VP), to the PS chain ends. As a result, the obtained membranes had controllable hydrophilic–hydrophobic properties. These membranes have shown high performance (5200 L $h^{-1}$ $m^{-2}$ for direct emulsions and 7400 L $h^{-1}$ $m^{-2}$ for reverse emulsions) for the separation and purification of water–oil emulsions (more than 95%). Based on the successful results of using protonated P4VP as a pH-responsive component of the PS-*g*-P4VP copolymer, deprotonated polyacrylic acid (PAA) was used as a pH-responsive polymer in this work. PAA as well as P4VP have a p$K_a$ lying in the low acid range (4.8 for PAA and 3.2 for P4VP).

This paper details, for the first time, a method for the fabrication of pH-sensitive membranes using UV-initiated RAFT graft copolymerization of ST and AA on PET TeMs. Through optimization of polymerization conditions, PS-*g*-PAA was successfully grafted onto PET TeMs, resulting in membranes with controlled wettability: at pH2 < p$K_{a_{PAA}}$ CA is 97° and at pH9 > p$K_{a_{PAA}}$ CA is 65°. These membranes have been successfully tested in the separation of direct and reverse two-component water–oil emulsions.

# 2 Materials and methods

## 2.1 Materials and chemicals

2-(Dodecylthiocarbonothioylthio)-2-methylpropionic acid as the RAFT-agent, and styrene (ST), acrylic acid (AA) monomers were acquired from Sigma Aldrich. Isopropyl alcohol (IPA), chloroform, benzene, *o*-xylene, benzophenone (BP), acetic acid, toluidine blue (TB), hydrochloric acid, *N*,*N*-dimethylformamide and sodium hydroxide have a purity of analytical grade ≥95%. Deionized water (18.2 MΩ) was prepared by Akvilon-D 301, PVC film (ISOLAB Laborgeraete GmbH, Germany), UV lamp (OSRAM Ultra Vitalux E27, Slovakia) was used in grafting, and a UV lamp (Osram Puritec, Germany) was used in photosensitization.

## 2.2 Preparation and modification of track-etched membranes

The preparation of PET TeMs at the DC-60 (Astana, Kazakhstan) has been a well-studied and established technology.[18,44] Fig. 1 illustrates the process of preparing and modifying the membrane, which is similar to the method described in article.[16]

23 μm thick PET films (Hostaphan® by Mitsubishi Polyester Film, Germany), were subjected to irradiation using Kr ions at an average energy of 1.75 MeV per nucleon to obtain cylindrical channels in the films. The pore density of the latent tracks (damaged areas) was $1.5 \times 10^6$ per $cm^2$. Photosensitization was carried out for 30 min under a UV lamp (Osram Puritec, Germany) with a wavelength of 254 nm and radiations of 12 W to enhance the track-etching process. In the etching stage, the polymer films were treated with 2.2 M NaOH for 10–12 min at a temperature of 84.5 °C leading to the formation of OH and COOH groups at the chain terminals in the damaged zones. This process facilitated the creation of pores in PET TeMs with diameters of 1.65 ± 0.07 μm.

The membranes were incubated for 24 h in a 5% BP solution in DMFA to activate the surface of PET TeMs. BP adsorbed on the membrane surface is a photosensitizer for radical UV-polymerization. The choice of 2-(dodecylthiocarbonothioylthio)-2-methylpropionic acid as a RAFT-agent is due to its suitability for styrene and acrylate types of monomers.[28,45] Preservation of thiocarbonylthio groups of the RAFT-agent at the chain ends of PS provides grafting of PAA, which allows the synthesis of PS-*g*-PAA block copolymer on the surface of PET TeMs.

The search for optimal conditions for grafting PAA was performed according to the following parameters: molar ratio of RAFT-agent to initiator (1 : 1 and 1 : 10), monomer concentration (36–720 mM), irradiation time (30–60 min), and distance from the UV source (7.5 and 10 cm). PS was grafted according to

 

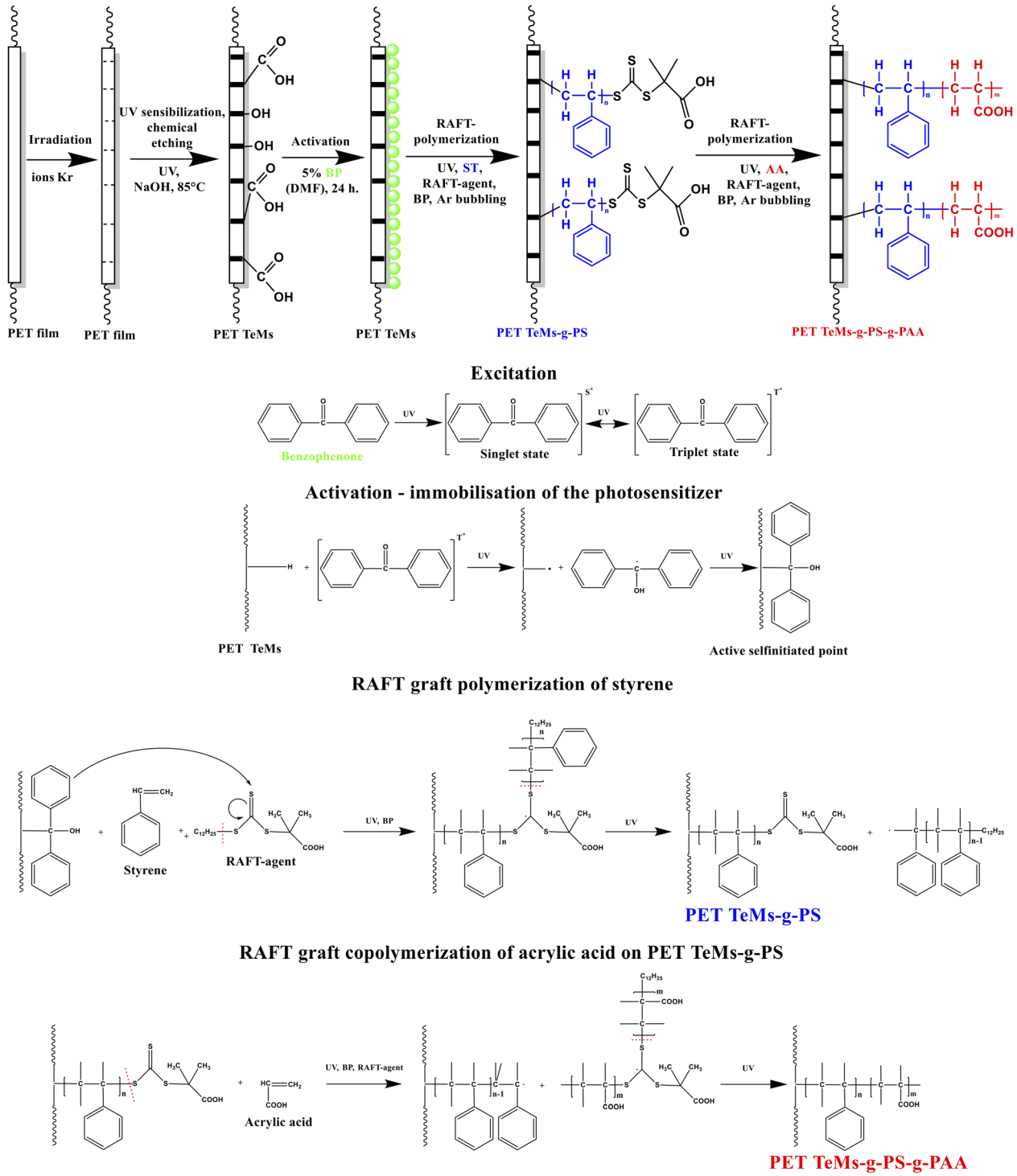


Fig. 1 Scheme and reaction pathways of preparation and modification of PET TeMs.

the optimal parameters already found in our previous work:[16] 172 mM (2 vol%), molar ratio RAFT-agent : initiator 1 : 10, distance from UV source 7.5 cm, and grafting time 60 min. The reaction mixture and the pristine sample were enclosed in a container, which was hermetically sealed with PVC film and was bubbled with argon for 10 min. Photopolymerization was performed under UV lamp (OSRAM Ultra Vitalux E27, Slovakia) with a wavelength of 315–400 nm and radiations of 13.6 W.

### 2.3. Methods of characterization

AFM was carried out on an NT-206 device (ALC Micro-testmachines, Belarus) to study the morphology (the average – $R_a$, nm and root mean square – $R_q$, nm) and local mechanical

properties (adhesion force $F_a$, nN, and elasticity modulus $E$, MPa) of the surfaces of micro- and nanometer-sized features. The average ($R_a$, nm) and root mean square ($R_q$, nm) roughness were obtained from 5 scanning areas (5 × 5 μm) and processed using Surface Explorer software. Local mechanical properties were calculated using the Johnson–Kendall–Roberts (JKR) model based on the silicon cantilever NSC 11 A ($k$ = 3 N m$^{-1}$) approach–departure curves to the sample surface.

A Specord-250 UV-vis spectrophotometer (Analytik Jena, Germany) was used to study terminal carboxyl groups on the membrane surface before and after modification. The concentration of terminal carboxyl groups was determined based on the sorption of TB dye (5 × 10$^{-4}$ M, pH 10) onto the membrane surface for 3 h and its desorption with acetic acid (50%). The absorbance of the desorbed TB dye was measured at 633 nm.

The grafting degree (DG) was evaluated by determining the mass of membranes before and after modification, according to eqn (1).[15,16,23]

$$DG = (m_2 - m_1)/m_1 \times 100\% \quad (1)$$

where DG—is the degree of grafting, $m_1$—is the weight of the membrane before grafting, and $m_2$—is the weight of the membrane after grafting.

The water CA was determined with DSA 100E (Kruss, Germany) using the lying drop method to characterize the wettability, adhesion, and adsorption of the sample surfaces. The surface free energy ($\omega$, mN m$^{-1}$) and its specific polar component ($\gamma^p$, mN m$^{-1}$) were calculated using the Owens, Wendt, Rabel, and Kelble method. This method uses the CA of two different liquids (polar and nonpolar) to determine the surface energy components of the membrane surface. Distilled water and diiodomethane were used as test liquids. The pH-responsivity of the membranes was determined from the response CA of PET-*g*-PS-*g*-PAA to changes in pH stimuli (Fig. 2).

The graft membranes were soaked in water at pH 2 and pH 9 for 30–120 min. Then the CA was measured.

TGA and derivative thermogravimetric (DTG) analyses were carried out to study the thermal stability and component composition of the copolymer on the instrument Pyris 1 TGA (PerkinElmer, USA) in the temperature range of 0 to 700 °C in a nitrogen atmosphere. A programmable temperature increase of 10 °C per minute was used.

FTIR spectra were recorded on a FTIR InfraLUM FT-08 spectrometer (Lumex) using an ATR attachment (Pike). All the measurements were conducted at a resolution of 2 cm$^{-1}$, and the number of scans was at least 20. The spectra obtained were processed in the SpectraLUM® suite. Peak areas were normalized with respect to the reference peak area at 1409 cm$^{-1}$, which applies to phenyl ring oscillations (C–H bending coupled with ring stretch).[46]

SEM-EDX analysis of the PET TeMs surface before and after modification was conducted using a Hitachi TM 3030 (Hitachi, Japan) instrument with a Bruker XFlash MIN SVE detector at 15 kV. Micro-images of 26 × 16 μm were obtained to examine the elemental composition (C, O, and S) and to monitor pore diameter using PhenomImageViewer software.

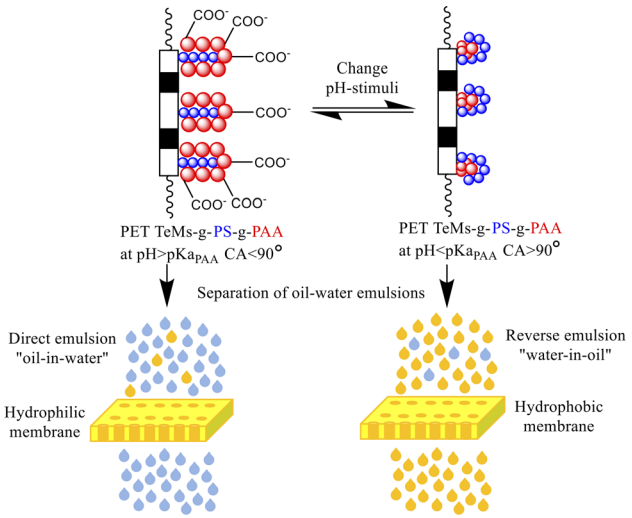


Fig. 2 Response of PET TeMs-*g*-PS-*g*-PAA to changes in pH stimuli due to the pH-sensitive component of PAA (p$K_{a_{PAA}}$ 4.8).

The strength of the membranes was assessed by the maximum pressure at which bursting occurred.

### 2.4. Testing of pH-responsive membranes in the separation of water–oil emulsions

Membranes with an area of 0.001256 m$^2$ were tested under vacuum pressure of 900 mbar on the VACSTAR Control Pump (IKA, Germany) on the filter unit presented in the previous work.[3] Depending on the type of emulsion, the membrane was soaked for 30–120 min in water at pH 2 for reverse emulsions and pH 9 for direct emulsions prior to testing (Fig. 2). Emulsions were prepared from two-component (dispersed and external) mixtures in a volume ratio of 1 : 100 on an Ultra-Turrax T18 disperser (IKA, Germany) at 24 000 rpm for 1 min. *o*-Xylene, chloroform, benzene, and "FASTROIL HPD SAE 40" motor oil were used as the oil components. The polar component was water at pH 2 for reverse emulsions as a dispersed component and at pH 9 for direct emulsions as an external component.

To evaluate the membrane performance, the filtered liquid flux was calculated using eqn (2), and the separation efficiency was calculated using eqn (3), as it is shown in the works.[3,15,16,30]

$$F = V/(S \times t) \quad (2)$$

$$R = (V_2/V_1) \times 100\% \quad (3)$$

where $F$—is the flux, L m$^{-2}$ h$^{-1}$; $V$—is the volume of external component that permeates through the membrane, L; $S$—is the filtration area of PET TeMs-*g*-PS-*g*-PAA, m$^2$; and $t$—is the flow time, h; $R$—is the separation efficiency, $V_1$—is the volume of dispersed component before separation; and $V_2$—is the volume of dispersed component after separation.

**2.4.1 Fouling and rejection of pH-responsive membranes in the separation of water–oil emulsions.** To evaluate membrane fouling and rejection, external component flux recovery and the total flux reduction factor were calculated

according to eqn (4) and (5).[47] The flux of the pure external component passing through the membrane was determined for the reverse emulsion separation of chloroform, benzene, and *o*-xylene, as well as for the direct emulsion separation of water with pH 9. Then, depending on the external component, the corresponding emulsions were separated. Subsequently, membranes were cleaned from the dispersed component by soaking them in a solution with pH 2 after the separation of reverse emulsions and in a solution with pH 9 after the separation of forward emulsions. Afterwards, the flux of the external component was determined again.

$$FR = (F_2/F_1) \times 100\% \quad (4)$$

$$TR = (1 - (F_0/F_1)) \times 100\% \quad (5)$$

where FR—is the flux recovery, %; TR—is the total flux reduction factor, %; $F_1$, $F_2$—fluxes of external components determined before and after emulsion separation, L $m^{-2}$ $h^{-1}$; $F_0$—emulsion separation flux, L $m^{-2}$ $h^{-1}$.

## 3 Results and discussion

UV-initiated RAFT copolymerization in live-chain mode was applied for grafting the PS-*g*-PAA block copolymer onto the surface of PET TeMs in two steps: RAFT-graft polymerization of ST and consequent RAFT-graft copolymerization of AA on PET TeMs-*g*-PS.

ST grafting was carried out by following the optimal conditions determined in the work:[16] ST concentration of 172 mM, molar ratio of RAFT-agent : initiator 1 : 10, distance to UV-lamp 7.5 cm and 60 min irradiation time. This receipt leads to the formation of a stable hydrophobic polystyrene layer with CA 97° ($DG_{PS}$ 2.6%) on the membrane surface with preservation of the pore structure. The presence of the active Z-group –$SC(CH_3)_2COOH$[48,49] in 2-(dodecylthiocarbonothioylthio)-2-methylpropionic acid at the chain ends of PS grafted to the surface of PET TeMs allows for the reversible addition–fragmentation of polymer chains and provides grafting of PAA (Fig. 1).

The following are the parameters of UV-initiated graft RAFT copolymerization of AA on PET TeMs-*g*-PS: concentration of AA (36–720 mM), molar ratio of RAFT agent: initiator (1 : 1, 1 : 10), grafting time (15–60 min) and distance from UV source (7.5, 10 cm) and their effect on water CA and $DG_{PAA}$ were studied. Irradiation for 120 min or more leads to degradation of the PET TeMs themselves,[15] accordingly, maximum irradiation was carried out for 60 min for PS grafting and 60 min for PAA grafting. Results are collected in Table 1.

The data in Table 1 shows that the $DG_{PAA}$ increases from 0.64 to 1.38% with increasing AA concentration from 36 to 72 mM and decreasing distance from UV lamp from 10 to 7.5 cm at 60 min of irradiation with a molar ratio of RAFT-agent : initiator = 1 : 1. However, the CA of the modified membranes did not respond to a change in the pH of the medium between 2 and 9, most probably due to the low level of grafting (1–1.5%) of PAA in view of the small concentration of AA and initiator in the reaction mixture.

Increasing the amount of initiator in the reaction mixture 10-fold and increasing the concentration of AA to 140 mM and 290 mM at a distance of 7.5 cm from the UV source and 60 min of irradiation results in a significant increase in the $DG_{PAA}$ to 3.96 and 3.28%, respectively. The membrane surface becomes more sensitive to pH stimuli, thus showing CA 86 and 82° at pH2 and 63 and 65° at pH9, respectively. Thus, sufficient hydrophobicity is not achieved.

The surface of the samples grafted with the PAA layer becomes brittle after irradiation at a UV lamp distance of 7.5 cm, a PAA concentration of 290 mM, and a molar ratio of

Table 1 Influence of AA graft polymerization conditions on contact angle and degree of grafting on PET TeMs-*g*-PS

| RAFT-agent : initiator, molar ratio | Distance to UV lamp, cm | Concentration of monomer, mM | Irradiation time, min | $DG_{PAA}$, ±0.05% | CA, ±3° | |
|---|---|---|---|---|---|---|
| | | | | | pH2 | pH9 |
| 1 : 1 | 7.5 | 36 | 60 | 0.72 | 101 | 101 |
| 1 : 1 | 7.5 | 72 | 60 | 1.62 | 100 | 100 |
| 1 : 1 | 10 | 36 | 60 | 0.64 | 96 | 96 |
| 1 : 1 | 10 | 72 | 60 | 1.38 | 99 | 99 |
| 1 : 10 | 7.5 | 36 | 60 | 1.53 | 99 | 99 |
| 1 : 10 | 7.5 | 72 | 60 | 1.94 | 101 | 95 |
| 1 : 10 | 7.5 | 140 | 60 | 3.96 | 86 | 63 |
| 1 : 10 | 7.5 | 290 | 60 | 3.28 | 82 | 65 |
| 1 : 10 | 10 | 36 | 60 | 1.2 | 97 | 94 |
| 1 : 10 | 10 | 72 | 60 | 1.45 | 100 | 95 |
| 1 : 10 | 10 | 140 | 60 | 1.67 | 95 | 83 |
| 1 : 10 | 10 | 290 | 60 | 1.72 | 96 | 78 |
| **1 : 10** | **10** | **430** | **60** | **2.6** | **97** | **65** |
| 1 : 10 | 10 | 580 | 60 | 2.76 | 86 | 70 |
| 1 : 10 | 10 | 720 | 60 | 2.92 | 83 | 68 |
| 1 : 10 | 10 | 430 | 15 | 0.52 | 78 | 63 |
| 1 : 10 | 10 | 430 | 30 | 0.87 | 91 | 71 |
| 1 : 10 | 10 | 430 | 45 | 1.95 | 93 | 68 |

Table 2 Burst strength for PET TeMs-*g*-PS-*g*-PAA as a function of distance from the UV lamp and AA concentration at a RAFT-agent : initiator molar ratio of 1 : 10 and irradiation time of 60 min

| Sample | Bursting pressure, kPa |
|---|---|
| Pristine PET TeMs | 286 |
| PET TeMs-*g*-PS, $DG_{PS} = 2.6\%$ | 243 |
| PET TeMs-*g*-PS-*g*-PAA, 7.5 cm, 140 mM, $DG_{PAA} = 3.96\%$ | 78 |
| PET TeMs-*g*-PS-*g*-PAA, 7.5 cm, 290 mM, $DG_{PAA} = 3.28\%$ | 62 |
| PET TeMs-*g*-PS-*g*-PAA, 10 cm, 290 mM, $DG_{PAA} = 1.72\%$ | 129 |
| **PET TeMs-*g*-PS-*g*-PAA, 10 cm, 430 mM, $DG_{PAA} = 2.6\%$** | **117** |
| PET TeMs-*g*-PS-*g*-PAA, 10 cm, 580 mM, $DG_{PAA} = 2.76\%$ | 86 |

Table 3 Influence of AA concentration at constant molar ratio of RAFT-agent : initiator 1 : 10, distance to UV-lamp 10 cm and irradiation time 60 min on the surface properties of PET TeMs-*g*-PS-*g*-PAA

| Sample, concentration of AA, $DG_{PAA}$ | CA at pH 7, ±3° | $\omega$, ±0.01 mN m$^{-1}$ | $\gamma^p$, ±0.01 mN m$^{-1}$ | $R_a$, nm | $R_q$, nm | $F_a$, ±5 nN | $E$, ±10 MPa |
|---|---|---|---|---|---|---|---|
| PET TeMs-*g*-PS-*g*-PAA, 36 mM, 1.2% | 97 | 33 | 1.3 | 32 | 43 | 38 | 192 |
| PET TeMs-*g*-PS-*g*-PAA, 72 mM, 1.45% | 98 | 43 | 0.3 | 19 | 25 | 46 | 146 |
| PET TeMs-*g*-PS-*g*-PAA, 290 mM, 1.72% | 87 | 29 | 4.4 | 21 | 29 | 45 | 124 |
| **PET TeMs-*g*-PS-*g*-PAA, 430 mM, 2.6%** | **75** | **38.5** | **7.5** | **9.6** | **14** | **83** | **110** |

RAFT-agent : initiator 1 : 10 for 60 min, which is confirmed by a significant decrease in the membrane tensile strength from 286 kPa for initial PET TeMs, 243 kPa for PET TeMs-*g*-PS, to 62 kPa for PET TeMs-*g*-PS-*g*-PAA. Grafting at a distance of 10 cm from the UV lamp under the same conditions shows less adverse effects, the strength decreases to a lesser extent to 129 kPa. The results of the tensile strength of the membranes are presented in Table 2.

With increasing AA concentration from 36 to 430 mM (at constant molar ratio of RAFT-agent : initiator 1 : 10, distance to UV-lamp 10 cm and irradiation time 60 min) $\omega$ and $\gamma^p$ increased from 32.79 to 38.53 mN m$^{-1}$ and from 1.3 to 7.5 mN m$^{-1}$, respectively, due to the increase of carboxyl groups of PAA on the surface of PET TeMs-*g*-PS ($\omega$ = 42 mN m$^{-1}$, $\gamma^p$ = 0.01 mN m$^{-1}$).[16] The influence of AA concentration on the surface properties is presented in Table 3.

AFM micrographs are presented in Fig. 3. Increasing $DG_{PAA}$ from 1.2 to 2.6% forms a smoother layer. $R_a$ and $R_q$ roughness values decrease from 32 to 9.6 and from 43 to 14 nN. $E$ vary within error limits for samples with $DG_{PAA}$ from 1.2 to 1.72%, further increasing the $DG_{PAA}$ to 2.6% lowers $F_a$ to 83 nN. $E$ is decreasing from 192 to 110 MPa with increasing concentrations of $DG_{PAA}$.

Decreasing the grafting time from 60 to 30 min at an AA concentration of 430 mM leads to a consistent decrease in the $DG_{PAA}$ from 2.6 to 0.87% and a decrease in the concentration of terminal carboxyl groups from 2.58 ± 0.7 to 1.72 ± 0.35 μmol g$^{-1}$ (Table 4), which leads to a decrease in the pH sensitivity of the samples according to corresponding CA values (Table 1).

Detection of –OH and C=O characteristic functional groups of PAA by FTIR-ATR spectroscopy was difficult because of the small amount of grafted polymer. But, after PAA grafting, the intensity of the peak corresponding to the absorption of C=O groups increases and shifts to 1713 cm$^{-1}$ (Fig. 4a). Also, the broadening of the peak at 2845 cm$^{-1}$ (PS-*g*-PET TeMs) corresponding to the stretching of C–H aliphatic groups was observed at 2862 cm$^{-1}$ after PAA grafting. The increase in methyl groups with increasing grafting time further indicates the grafting of PAA on PET TeMs-*g*-PS (Fig. 4c).

Further reduction of irradiation time to 15 min also lowers the $DG_{PAA}$ to 0.52%. Despite this, the concentration of terminal carboxyl groups increases to 2.86 ± 0.28 μmol g$^{-1}$, causing the CA of these samples to decrease at pH2 78° and at pH9 63°. This deviation of CA in relation to the $DG_{PAA}$ has been attributed to the presence of the COOH group of the RAFT-agent to a greater extent on the membrane surface due to the short irradiation time, indirectly confirmed by the increase in the peak area at 3567 cm$^{-1}$ (Fig. 4b), corresponding to the free vibrations of the OH groups in the COOH groups in the FTIR-ATR spectra of the modified samples from 0.025 at 60 min of irradiation to 0.102 at 15 min of irradiation. The FTIR-ATR spectra of the samples are presented in Fig. 4. Thus, with decreasing irradiation time, the presence of RAFT-agent becomes more effective on the membrane surface. Additional justification for this finding is the minimal response of CA even at the highest concentration of COOH (2.86 ± 0.28 μmol g$^{-1}$) at pH changes in the pH-response range of PAA.

FTIR-ATR spectra of the membranes before and after grafting consist of characteristic PET absorption peaks: for the ester C=O groups 1714 cm$^{-1}$, for aromatic ring bending CH 1409 cm$^{-1}$, bending CCC 1017 cm$^{-1}$, stretching CC 872 cm$^{-1}$, for bending $CH_2$ groups 1340 cm$^{-1}$ and 1244 cm$^{-1}$, for stretching C–O groups 971 cm$^{-1}$; absorption peaks of PS: for bending C–H out-of-plane 699 cm$^{-1}$ and 759 cm$^{-1}$, for

 

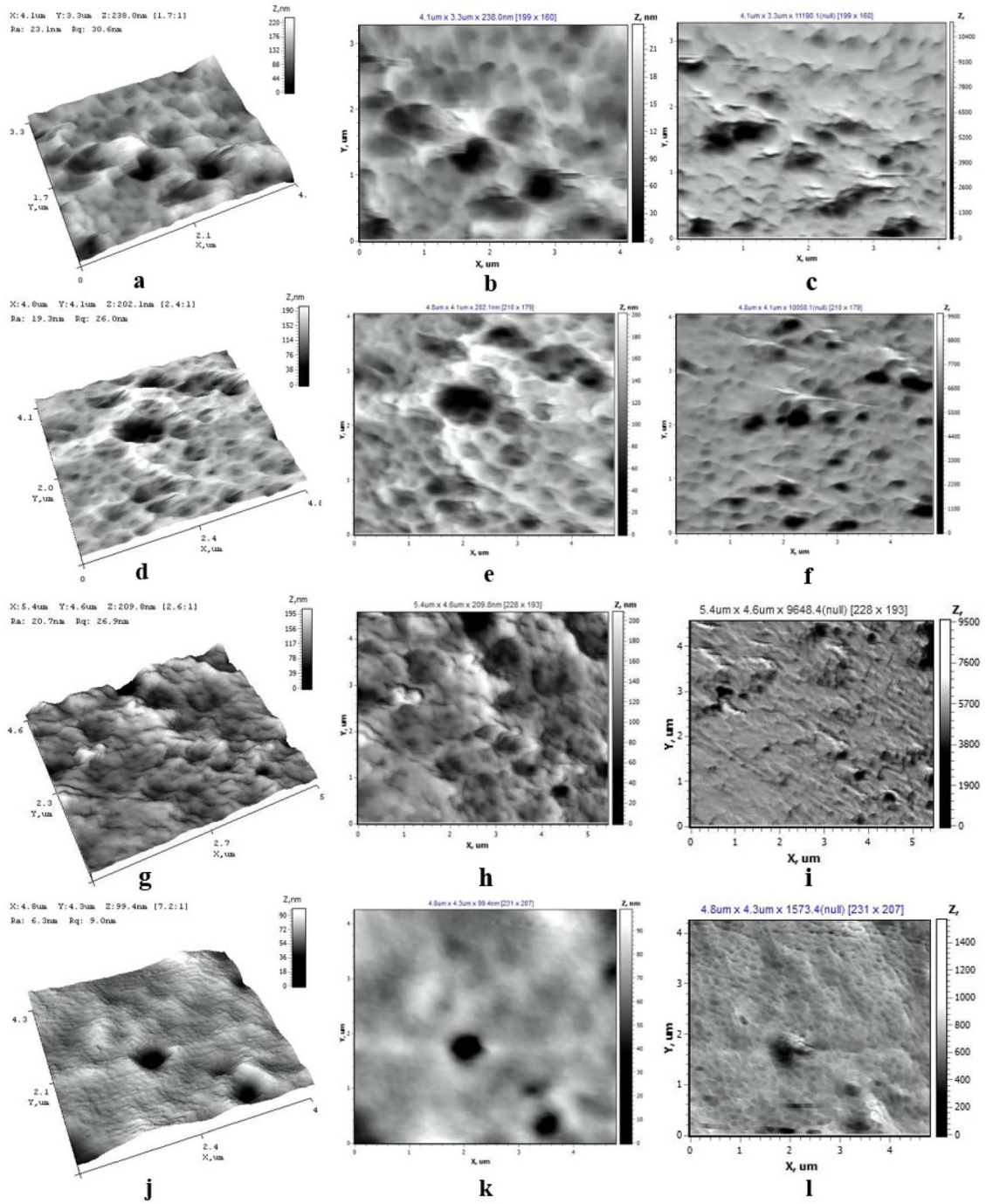


Fig. 3 AFM images sized 5 × 5 μm$^2$ of PET TeMs-*g*-PS-*g*-PAA, grouped by type: 3D (a, d, g and j), topographic (b, e, h and k), and torsion (c, f, i and l). Samples are grafted under varying conditions: AA concentration 36 mM and $DG_{PAA}$ 1.2% (a–c); 72 mM and 1.45% (d–f); 290 mM and 1.72% (g–i); 430 mM and 2.6% (j–l). All samples were prepared with a constant molar ratio of RAFT-agent to initiator (1 : 10), at a distance of 10 cm from the UV lamp, and an irradiation time of 60 min.

stretching C=C aromatic 1601 cm$^{-1}$, 1492 cm$^{-1}$ and 1452 cm$^{-1}$. Belonging of the absorption peaks to PET-*g*-PS, presented in Fig. 4, is reliable, as they agree on wave numbers in articles.[46,50,51]

Thus, the optimal parameters of UV-initiated RAFT graft copolymerization of AA on PET TeMs-*g*-PS can be given as:

– Distance from UV source – 10 cm,
– Molar ratio of RAFT-agent to initiator – 1 : 10,
– AA concentration – 430 mM,
– Irradiation time 60 min.

Under these experimental conditions the $DG_{PAA}$ was 2.6%, at which the maximum response of the membrane surface to changes in pH environment was observed at pH2 CA 97° and at pH9 65°. Further increase in AA concentration up to 720 mM at

Table 4 Effect of irradiation time on the number of carboxyl groups on PET TeMs-*g*-PS-*g*-PAA surface at AA concentration of 430 mM, molar ratio of RAFT-agent : initiator 1 : 10, and distance to UV lamp 10 cm

| Sample, irradiation time, $DG_{PAA}$ | Concentration of COOH, μmol $g^{-1}$ | $A_{3567}/A_{1410}$ |
|---|---|---|
| Pristine PET TeMs | 0.53 ± 0.03 | 0.002 |
| PET TeMs-*g*-PS | 0.8 ± 0.03 | 0.018 |
| PET TeMs-*g*-PS-*g*-PAA, 15 min, 0.52% | 2.86 ± 0.28 | 0.102 |
| PET TeMs-*g*-PS-*g*-PAA, 30 min, 0.87% | 1.72 ± 0.35 | 0.034 |
| PET TeMs-*g*-PS-*g*-PAA, 45 min, 1.95% | 2.26 ± 0.11 | 0.034 |
| **PET TeMs-*g*-PS-*g*-PAA, 60 min, 2.6%** | **2.58 ± 0.17** | **0.025** |

optimum parameters results in decrease in CA at pH2 83° and at pH9 68° (Table 1), since the grafted PAA layer dominates $DG_{PAA}$ = 2.92% over the PS layer $DG_{PS}$ = 2.6%.

According to EDX-SEM data, carbon, oxygen and sulphur are present on the surface of PET TeMs-*g*-PS-*g*-PAA after grafting under optimal conditions ($DG_{PAA}$ = 2.6%) in atomic contents of 77, 22 and 0.28%, respectively, and the pore diameter decreases from 1.65 ± 0.08 (PET TeMs) to 1.51 ± 0.04 μm. The EDX mapping shows a uniform distribution of C, O and S elements on the membrane surface. Sulphur is coming from the end groups of the RAFT agent. The images obtained by EDX-SEM are shown in Fig. 5.

The TGA and DTG curves of PET TeMs grafted with PS-*g*-PAA under optimal conditions are shown in Fig. 6. The thermogram of pristine PET TeMs presents a single-phase stage decomposition process with maximum decomposition at 463 °C corresponding to a weight loss of 52% (Fig. 6b). 381 °C is the onset of decomposition, with final weight losses of 99% for PET TeMs, 98% for PET TeMs-*g*-PS, and 97% for PET TeMs-*g*-PS-*g*-PAA. After grafting of PS, the weight also decreases smoothly to 47% at 465 °C. The DTG curve reveals a small degradation peak at 447 °C with a weight loss of 74% (Fig. 6c), which relates to polystyrene chain breakage.[52,53] The grafting of PAA leads to a decrease in thermal stability, the degradation maximum corresponds to a weight loss of 45%; and the mass continues to decrease with a small hike in the region of 509–595 °C (Fig. 6d). A similar trend with a smooth transition in weight loss at 503 is presented in ref. 54. The mass change at 129 °C after grafting PS-*g*-PAA can be attributed to the escape of water or other volatile impurities adsorbed on the membrane surface.[55]

The results of testing pH-responsive PET TeMs-*g*-PS-*g*-PAA membranes with pore diameters of 1.52 nm in the separation of direct and reverse two-component water–oil emulsions are presented in Fig. 7. The performance of the membranes in terms of fluxes and separation efficiency was compared with smart membranes exhibiting switchable wettability obtained by other research groups and presented in Table 5.

The *F* (flux) for benzene–water, *o*-xylene–water, and motor water–oil direct emulsions show high stability for 10 separation cycles as they deviate from the average *F* values within 10%: 247 ± 24, 573 ± 57, and 47 ± 3 L $m^{-2}$ $h^{-1}$, respectively. Since water with pH 9 in the composition of direct emulsions allows to

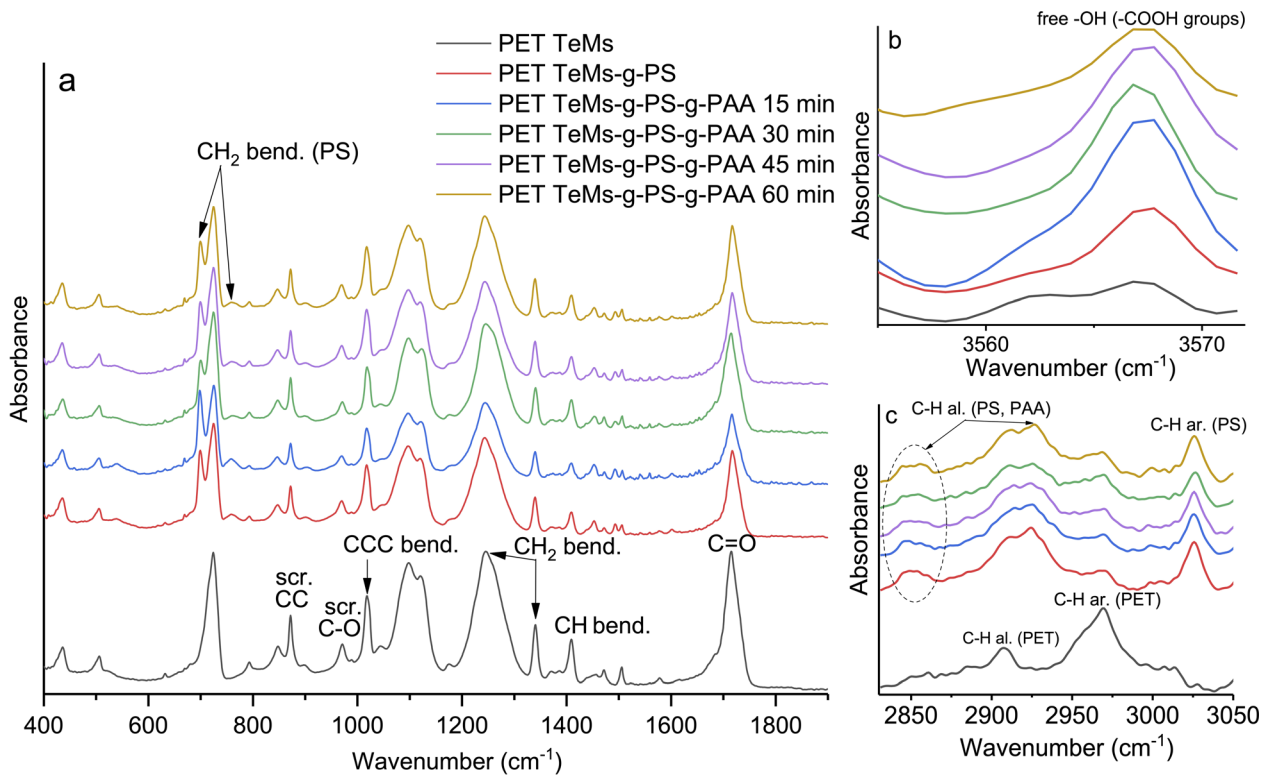


Fig. 4 FTIR spectra of PET TeMs-*g*-PS-*g*-PAA as a function of irradiation time at constant AA concentration 430 mM, molar ratio of RAFT-agent : initiator 1 : 10, and distance to UV lamp 10 cm in the range of 400–1800 $cm^{-1}$ (a), 3560–3570 $cm^{-1}$ (b), 2825–3050 $cm^{-1}$ (c).

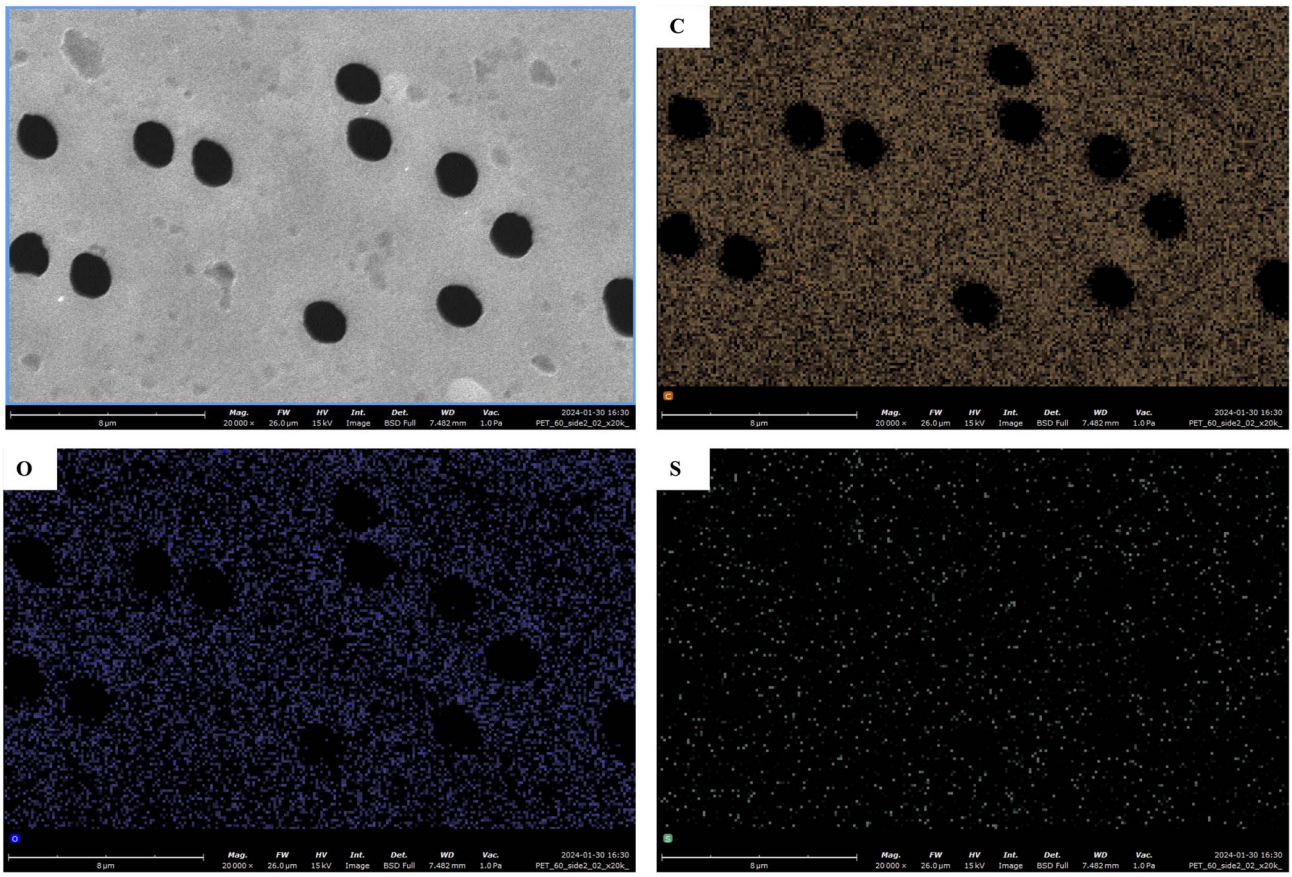


Fig. 5 SEM and EDX-mapping pictures of C, O, and S elements PET TeMs-*g*-PS-*g*-PAA produced at AA concentration 430 mM, molar ratio of RAFT-agent : initiator 1 : 10, distance to UV lamp 10 cm, and irradiation time 60 min ($DG_{PAA}$ = 2.6%).

maintain the hydrophilicity of the membrane. The separation *F* for the direct chloroform–water emulsion is less stable due to the higher value of the average separation *F* of 2055 ± 230 L $m^{-2}$ $h^{-1}$, and, consequently, the spread is larger compared to the lower separation *F* (Fig. 7a).

On the contrary, the separation *F* for reverse emulsions is less stable as compared to direct emulsions (Fig. 7). The decrease in the separation *F* of reverse emulsions is caused by the decrease in the emulsion pH by organic components, which leads to an increase in negatively charged $COO^-$ groups on the membrane surface. A decrease in CA concurrently weakens the retention of water droplets. Due to the presence of water at pH 2 in the composition of reverse emulsions, the separation efficiency *R* is maintained at a high level. The separation F decreases sharply after the first separation cycle for reverse emulsions with benzene from 1700 to 550 L $m^{-2}$ $h^{-1}$ and chloroform from 1400 to 420 L $m^{-2}$ $h^{-1}$ (Fig. 7b) due to membrane surface fouling with the accumulation of organic components during reuse, as the fluxes decrease to a lesser extent of ±50 L $m^{-2}$ $h^{-1}$ after washing the membranes in isopropyl alcohol. A similar reduction in separation *F* for chloroform–water reverse emulsions was presented in our previous work for hydrophobic PET TeMs-TCOS (pore diameter 350 nm, pressure 800 mbar) and PET TeMs-*g*-SM (pore diameter 3.05 μm, pressure 900 mbar) from 1000 to 780 L $m^{-2}$ $h^{-1}$ and from 4000 to 3350 L $m^{-2}$ $h^{-1}$, respectively.[3,15] The separation *F* of the more viscous *o*-xylene from water is less than for chloroform and benzene in reverse emulsions.

The separation *F* of two-component emulsions depends on the viscosity and density of the dispersed component and the external component, which influence emulsion stability.[56,57] The greater the difference in density between the dispersed component and the external component and the lower the viscosity of the dispersed component compared to the external component, the less stable the emulsion, and the higher the separation *F*. Thus, the separation flux of direct emulsions decreases with decreasing density of the organic components chloroform, *o*-xylene, and benzene. FASTROIL HPD SAE 40 motor oil with a density of 886 kg $L^{-1}$ and a dynamic viscosity of 89 mPa s at 20 °C is more viscous with a complex composition including base oils and various additives that can create additional barriers to mixing with water compared to the pure solvents: benzene, *o*-xylene, and chloroform. Despite the low separation *F* values, the engine oil–water emulsion is stable. Above 10 cycles, *R* for the direct and reverse emulsions was more than 94 ± 5% and 97 ± 1%, respectively. The pH-responsive PET TeMs-*g*-PS-*g*-PAA membranes (pore diameter 1.51 ± 0.04 μm, CA at pH2 – 97°, pH9 – 65°) are inferior in *F* and *R* for both direct and reverse emulsions to PET TeMs-*g*-PS-*g*-P4VP membranes

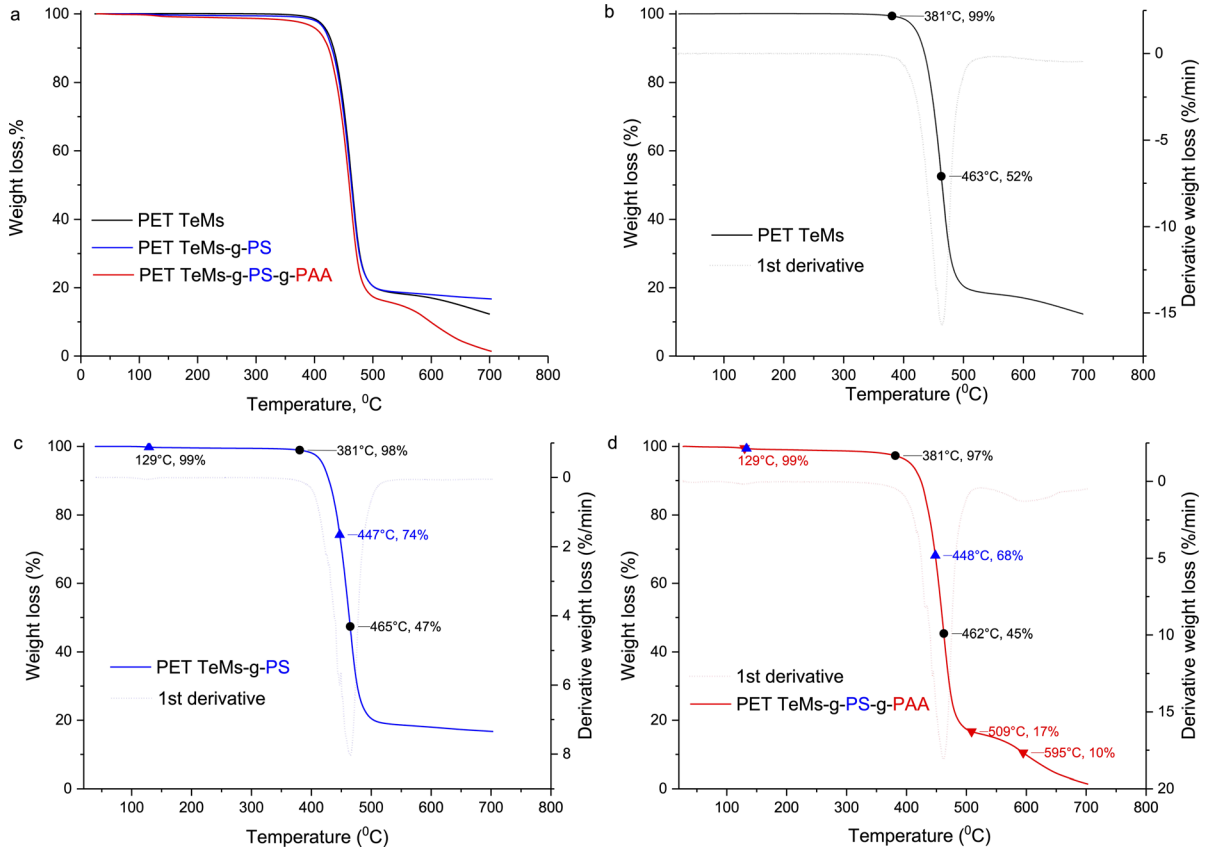


Fig. 6 TGA thermograms for the pristine PET TeMs, PET TeMs-*g*-PS, and PET TeMs-*g*-PS-*g*-PAA (a) and TGA-DTG curves for the pristine PET TeMs (b), PET TeMs-*g*-PS $DG_{PS} = 2.6\%$ (c), PET TeMs-*g*-PS-*g*-PAA $DG_{PAA} = 2.6\%$ (d).

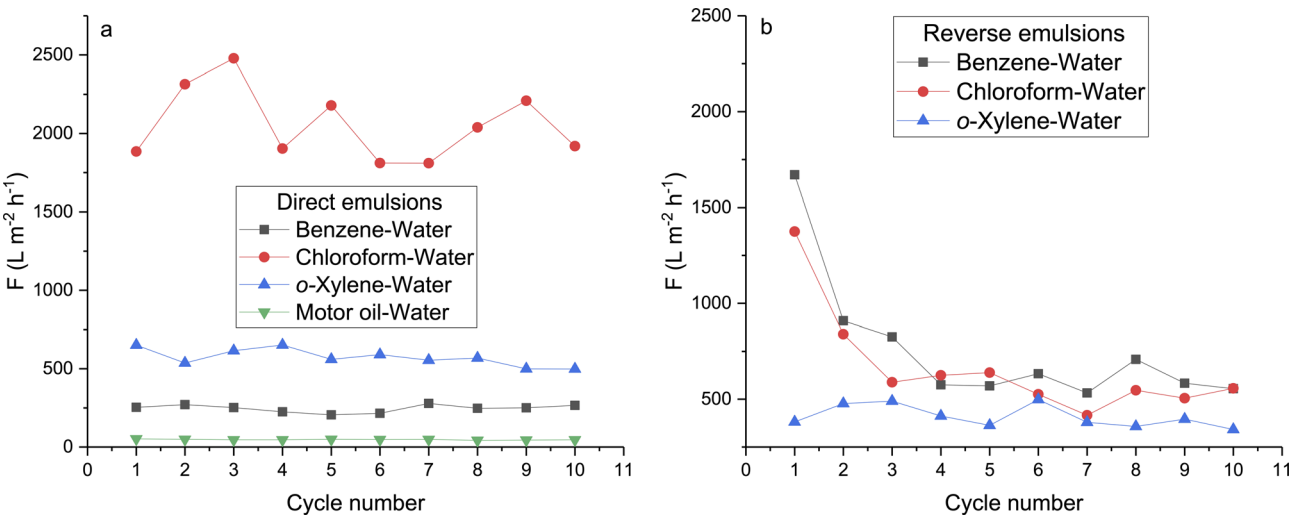


Fig. 7 The fluxes of pH-responsive PET TeMs-*g*-PS-*g*-PAA for direct (a) and reverse (b) emulsions at 900 mbar.

(pore diameter $1.7 \pm 0.1$ μm, CA at pH9 – 95°, at pH2 – 58°), due to the smaller pore diameter and lower response to pH changes.

The evaluation of contamination and rejection of PET TeMs-*g*-PS-*g*-PAA by flux recovery and total flux reduction factor, depending on the type and composition of the emulsion to be separated, is presented in Table 6.

The fouling and rejection resistance of PET TeMs-*g*-PS-*g*-PAA is high in the separation of chloroform-in-water direct emulsion and water-in-benzene reverse emulsion, as FR is recovered by 82% and 96%, respectively, and TR is reduced by 22% and 12%, respectively. Significant membrane fouling occurs in the separation of benzene-in-water and *o*-xylene-in-water direct

Table 5 Comparison of PET TeMs-*g*-PS-*g*-PAA with smart materials exhibiting switchable wettability for separating direct and reverse emulsions in terms of flux and efficiency of separation emulsions

| Material | Stimuli | Response | Emulsion | Pressure | $F$, L m$^{-2}$ h$^{-1}$ | $R$, % | Ref. |
|---|---|---|---|---|---|---|---|
| PET TeMs-*g*-PS-*g*-PAA | Change pH above and below p$K_{a_{PAA}}$ = 4.8 | Hydrophilicity pH > p$K_{a_{PAA}}$ | *o*-Xylene-in-water | 900 mbar | 650–500 | 96 ± 2 | This work |
| | | | Benzene- in-water | | 280–210 | 96 ± 3 | |
| | | | Chloroform-in-water | | 2500–1800 | 94 ± 5 | |
| | | | Motor oil–water | | 52–43 | 92 ± 3 | |
| | | Hydrophobicity pH < p$K_{a_{PAA}}$ | Water-in-benzene | | 1700–550 | 99 ± 1 | |
| | | | Water-in-chloroform | | 1400–420 | 97 ± 1 | |
| | | | Water-in-*o*-xylene | | 500–340 | 99 ± 1 | |
| PET TeMs-*g*-PS-*g*-P4VP | Change pH above and below p$K_{a_{P4VP}}$ | Hydrophilicity pH < p$K_{a_{P4VP}}$ | Cetane-in-water | 900 mbar | 5200–2550 | 97 ± 1 | 16 |
| | | Hydrophobicity pH > p$K_{a_{P4VP}}$ | Water-in-hexane | | 7400–6300 | 99 ± 1 | |
| CC-coated PVDF | Ethanol washing + drying/drying + ethanol washing | Superoleophobicity Superhydrophobicity | Water-in-hexane Kerosine-in-water | 850 mbar | 50–110 60–75 | 99 99 | 37 |
| SNP/DA-$TiO_2$/PI | Change pH, ammonia-vapor | Superhydrophobicity at pH 6.5 | Chloroform–water (1 : 1 by vol.) | LEP of chloroform | 5000 | 99 | 36 |
| | | Superhydrophilicity at pH 12 or ammonia-vapor | Chloroform–water (1 : 1 by vol.) | LEP of water | 5000 | 99 | |

Table 6 Flux recovery and total flux reduction factor of PET TeMs-*g*-PS-*g*-PAA in the separation of reverse and direct emulsions of different compositions

| Emulsion | FR, % | TR, % |
|---|---|---|
| Water-in-*o*-xylene | 83 | 76 |
| Water-in-chloroform | 96 | 46 |
| Water-in-benzene | 96 | 12 |
| *o*-Xylene-in-water | 75 | 81 |
| Benzene-in-water | 81 | 77 |
| Chloroform-in-water | 82 | 22 |

emulsions and water-in-*o*-xylene reverse emulsions, as their TR is reduced by 81, 77, and 76%, but nevertheless, after washing these membranes in pH 9 (direct emulsions) and pH 2 (reverse emulsions), their FR is recovered by 75, 81 and 83%, respectively.

The resulting pH-responsive PET TeMs-*g*-PS-*g*-PAA can be successfully applied to the separation of both direct and reverse emulsions. In contrast to common practice, where membranes are only used to separate a specific type of emulsion, membranes obtained in this work are versatile and function effectively in both directions. High $F$ and $R$ of separation were achieved for direct chloroform–water 2500 L m$^{-2}$ h$^{-1}$, and reverse emulsions of benzene–water 1700 L m$^{-2}$ h$^{-1}$ and chloroform–water 1400 L m$^{-2}$ h$^{-1}$. Also, membranes are less fouled during the separation of these emulsions (high FR values of 96 and 83%, low TR values of 12 and 22%). The developed membranes were comparable to other smart membranes in terms of flux and emulsion separation efficiency reported in the literature.

## 4 Conclusions

In this study, pH-sensitive membranes were obtained by UV-initiated RAFT graft copolymerization of hydrophobic ST and hydrophilic AA on the surface of PET TeMs. The pH sensitivity is due to the presence of carboxyl groups of PAA, which contribute to the CA in response to changes in the environmental pH above or below the p$K_{a_{PAA}}$ = 4.8. The highest membrane response to pH change was recorded for the membranes synthesized in the following conditions: distance from UV source – 10 cm, molar ratio of RAFT-agent to initiator – 1 : 10, concentration of monomer – 430 mM and irradiation time of 60 min. In basic environment at pH9 the CA of membrane surface is 65° and in acidic environment at pH2 on the contrary CA is 97°. The obtained pH-sensitive PET TeMs-*g*-PC-*g*-PAAs with switchable hydrophilicity/hydrophobicity were successfully tested in the separation of several water-in-oil emulsions with efficiency of more than 90% and flux of separation for direct emulsions for 2500 L m$^{-2}$ h$^{-1}$ (chloroform-in-water) and for reverse emulsions for 1700 L m$^{-2}$ h$^{-1}$ (water-in-benzene). The membranes are also characterized by antifouling properties with a chloroform flux recovery of 96% and a slight decrease in total flux reduction factor of 12% in the separation of water-in-chloroform reverse emulsion.

Thus, in this work, the surface properties of PET TeMs with regular pore diameter and small thickness have been enhanced

by a simple method leading to controlled wettability by changing the pH of the environment. This type of membrane seems to be versatile, as it has the potential to the separate two types of water–oil emulsions.

## Author contributions

Conceptualization, I. V. K., I. B. M. and O. G.; methodology, I. V. K., I. B. M.; validation, I. B. M., N. Zh. and S. A. C.; investigation, I. B. M., N. Zh. and A. B. Y.; data curation, S. A. C., Z. K. Z.; writing—original draft preparation, I. B. M.; writing—review and editing, O. G., G. B. M., M. V. Z.; supervision, I. B. M. and I. V. K.; project administration, I. B. M.; funding acquisition, I. B. M., I. V. K. All authors have read and agreed to the published version of the manuscript.

## Conflicts of interest

There are no conflicts to declare.

## Acknowledgements

The article was prepared as part of the implementation of the scientific project of the grant funding Project "Young Scientist" for 2022–2024 of the Science Committee of the Ministry of Science and Higher Education of the Republic of Kazakhstan AP14972816 "Stimuli-responsive track-etched membranes for separation of water–oil emulsions" and BRFFR T22MS-029 (contract dated May 4, 2022).

## References

1 I. B. Ivshina, M. S. Kuyukina, A. V. Krivoruchko, A. A. Elkin, S. O. Makarov, C. J. Cunningham, T. A. Peshkur, R. M. Atlas and J. C. Philp, *Environ. Sci.: Process. Impacts*, 2015, **17**, 1201–1219.
2 N. Zhang, X. Yang, Y. Wang, Y. Qi, Y. Zhang, J. Luo, P. Cui and W. Jiang, *J. Environ. Chem. Eng.*, 2022, **10**, 107257.
3 I. V. Korolkov, A. R. Narmukhamedova, G. B. Melnikova, I. B. Muslimova, A. B. Yeszhanov, Z. K. Zhatkanbayeva, S. A. Chizhik and M. V. Zdorovets, *Membranes*, 2021, **11**(8), 637.
4 X. Li, H. Xu, J. Liu, J. Zhang, J. Li and Z. Gui, *Sep. Purif. Technol.*, 2016, **165**, 101–106.
5 D. Jang, J. Lee and A. Jang, *Chemosphere*, 2023, **313**, 137596.
6 M. Liu, L. Shen, J. Wang, Y. Ding, Y. Zhou and F. Liu, *J. Membr. Sci.*, 2022, **660**, 120876.
7 N. Zhang, X. Yang, Y. Wang, Y. Qi, Y. Zhang, J. Luo, P. Cui and W. Jiang, *J. Environ. Chem. Eng.*, 2022, **10**, 107257.
8 H. H. Tseng, J. C. Wu, Y. C. Lin and G. L. Zhuang, *J. Membr. Sci.*, 2018, **559**, 148–158.
9 W. Jankowski, G. Li, W. Kujawski and J. Kujawa, *Sep. Purif. Technol.*, 2022, **302**, 122101.
10 X. Lin, B. Li, Z. Liu, H. Yin, C. Zheng, Y. Li, X. Wu, H. Wu and H. Zhang, *Sep. Purif. Technol.*, 2024, **334**, 126017.
11 R. He, Y. Wu, Y. Liu, L. Luo, H. Xiao, C. Huang, X. Wang, Z. Zeng, J. He and Y. Zhang, *Prog. Org. Coat.*, 2024, **188**, 108192.
12 M. Ghorbani, M. Hassan Vakili and E. Ameri, *Mater. Today Commun.*, 2021, **28**, 102560.
13 O. Ejeromedoghene, S. Abesa, E. Akor and A. O. Omoniyi, *Mater. Today Commun.*, 2023, **35**, 106063.
14 M. Liu, L. Shen, J. Wang, Y. Ding, Y. Zhou and F. Liu, *J. Membr. Sci.*, 2022, **660**, 120876.
15 A. B. Yeszhanov, I. B. Muslimova, G. B. Melnikova, A. S. Petrovskaya, A. S. Seitbayev, S. A. Chizhik, N. K. Zhappar, I. V. Korolkov, O. Güven and M. V. Zdorovets, *Polymers*, 2022, **14**, 3015.
16 I. B. Muslimova, Z. K. Zhatkanbayeva, D. D. Omertasov, G. B. Melnikova, A. B. Yeszhanov, O. Güven, S. A. Chizhik, M. V. Zdorovets and I. V. Korolkov, *Membranes*, 2023, **13**, 523.
17 A. B. Yeszhanov, I. V. Korolkov, S. S. Dosmagambetova, M. V. Zdorovets and O. Güven, *Polymers*, 2021, **13**(15), 2520.
18 P. Apel, *Radiat. Meas.*, 2001, **34**, 559–566.
19 Z. Xiong, H. Yu and X. Gong, *Langmuir*, 2022, **38**, 8708–8718.
20 Q. Xiong, H. Chen, Q. Tian, X. Yue, F. Qiu, T. Zhang and A. B. Wang, *J. Environ. Chem. Eng.*, 2022, **10**, 108459.
21 H. Chen, Z. Zuo, Q. Tian, S. Xue, F. Qiu, X. Peng and T. Zhang, *J. Cleaner Prod.*, 2023, **396**, 136502.
22 H. N. Doan, P. Phong Vo, K. Hayashi, K. Kinashi, W. Sakai and N. Tsutsumi, *J. Environ. Chem. Eng.*, 2020, **8**, 103921.
23 N. Parmanbek, D. S. Sütekin, M. Barsbay, A. A. Mashentseva, D. A. Zheltov, N. A. Aimanova, Z. Y. Jakupova and M. V. Zdorovets, *Polymers*, 2022, **14**, 4026.
24 M. Barsbay, O. Güven, H. Bessbousse, T. L. Wade, F. Beuneu and M. C. Clochard, *J. Membr. Sci.*, 2013, **445**, 135–145.
25 X. Tian, J. Ding, B. Zhang, F. Qiu, X. Zhuang and Y. Chen, *Polymers*, 2018, **10**, 318.
26 J. Luo, D. Cheng, M. Li, M. Xin, W. Sun and W. Xiao, *Adv. Polym. Technol.*, 2020, **2020**, 3695234.
27 D. J. Keddie, *Chem. Soc. Rev.*, 2014, **43**, 496–505.
28 G. Moad, E. Rizzardo, and S. H. Thang, *Controlled Radical Polymerization Guide, ATRP, RAFT, NMP*, **https://www.sigmaaldrich.com/KZ/en/technical-documents/technical-article/materials-science-and-engineering/polymer-synthesis/micro-review-of-reversible-addition-fragmentation-chain-transfer-raft-polymerization?utm_source=google&utm_medium=cpc&utm_campaign=10193651930&utm_content=101663337573&gclid=CjwKCAjw57exBhAsEiwAaIxaZvlU0PDDGpinS1Q8ZU0eFJC3FADxQGGbtLibZXP–sUW60ZE–gpQRoCNoIQAvD_BwE**.
29 D. Wandera, S. R. Wickramasinghe and S. M. Husson, *J. Membr. Sci.*, 2010, **357**, 6–35.
30 P. Dansawad, Y. Yang, X. Li, X. Shang, Y. Li, Z. Guo, Y. Qing, S. Zhao, S. You and W. Li, *Adv. Membr.*, 2022, **2**, 100039.
31 O. Ejeromedoghene, S. Abesa, E. Akor and A. O. Omoniyi, *Mater. Today Commun.*, 2023, **35**, 106063.
32 J. J. Li, Y. N. Zhou and Z. H. Luo, *Prog. Polym. Sci.*, 2018, **87**, 1–33.

33 D. L. Keshebo, H. F. Darge, C. C. Hu, H. C. Tsai, C. J. Su, Y. M. Sun, W. S. Hung, C. F. Wang, K. R. Lee and J. Y. Lai, *J. Membr. Sci.*, 2022, **664**, 121080.
34 H. Sun, J. Guan, H. Chai, K. Yu, L. Qu, X. Zhang and G. Zhang, *Biosens. Bioelectron.*, 2024, **251**, 116080.
35 P. Kumari, N. Bahadur, X. A. Conlan, X. Zeng, L. Kong, L. A. O'Dell, A. Sadek, A. Merenda and L. F. Dumée, *Chem. Eng. J.*, 2023, **452**, 139374.
36 W. Ma, S. K. Samal, Z. Liu, R. Xiong, S. C. De Smedt, B. Bhushan, Q. Zhang and C. Huang, *J. Membr. Sci.*, 2017, **537**, 128–139.
37 Y. Long, Y. Shen, H. Tian, Y. Yang, H. Feng and J. Li, *J. Membr. Sci.*, 2018, **565**, 85–94.
38 Q. Qi, Q. Shen, J. Geng, W. An, Q. Wu, N. Wang, Y. Zhang, X. Li, W. Wang, C. Yu and L. Li, *Adv. Colloid Interface Sci.*, 2024, **324**, 103087.
39 J. Wu, W. Xue, Z. Yun, Q. Liu and X. Sun, *Mater. Today Bio*, 2024, **25**, 100998.
40 A. Kayani, A. Raza, J. Si, D. Dutta, Q. Zhou and Z. Ge, *Biomacromolecules*, 2023, **24**, 4622–4645.
41 A. Balafouti and S. Pispas, *Pharmaceutics*, 2023, **15**, 1198.
42 Y. Zhang and X. Gong, *Giant*, 2023, **14**, 100157.
43 O. Ejeromedoghene, S. Abesa, E. Akor and A. O. Omoniyi, *Mater. Today Commun.*, 2023, **35**, 106063.
44 A. Kozlovskiy, D. Borgekov, I. Kenzhina, M. Zdorovets, I. Korolkov, E. Kaniukov, M. Kutuzau and A. Shumskaya, *Springer Proc. Phys.*, 2019, **221**, 461–479.
45 D. J. Keddie, *Chem. Soc. Rev.*, 2014, **43**, 496–505.
46 M. Drobota, Z. Persin, L. F. Zemljic, T. Mohan, K. Stana-Kleinschek, A. Doliska, M. Bracic, V. Ribitsch, V. Harabagiu and S. Coseri, *Cent. Eur. J. Chem.*, 2013, **11**, 1786–1798.
47 H. S. Fahmy, R. Abouzeid, M. S. A. El-sadek, G. T. Abdel-Jaber, W. Y. Ali and H. M. Mousa, *Cellulose*, 2023, **30**, 5871–5893.
48 J. Chiefari, R. T. A. Mayadunne, C. L. Moad, G. Moad, E. Rizzardo, A. Postma, M. A. Skidmore and S. H. Thang, *Macromolecules*, 2003, **36**(7), 2273–2283.
49 S. J. Stace, G. Moad, C. M. Fellows and D. J. Keddie, *Polym. Chem.*, 2015, **6**, 7119–7126.
50 J. Fang, Y. Xuan and Q. Li, *Sci. China: Technol. Sci.*, 2010, **53**, 3088–3093.
51 I. V. Korolkov, A. B. Yeszhanov, M. V. Zdorovets, Y. G. Gorin, O. Güven, S. S. Dosmagambetova, N. A. Khlebnikov, K. V. Serkov, M. V. Krasnopyorova, O. S. Milts and D. A. Zheltov, *Sep. Purif. Technol.*, 2019, **227**, 115694.
52 M. Abd Al- and H. Abood, *Aust. J. Basic Appl. Sci.*, 2013, **7**, 746–750.
53 S. E. Hachani, A. A. Wis, Z. Necira, N. Nebbache, A. Meghezzi and G. Ozkoc, *Acta Chim. Slov.*, 2018, **65**, 646–651.
54 P. Mente, T. N. Phaahlamohlaka, V. Mashindi and N. J. Coville, *J. Mater. Sci.*, 2021, **56**, 2113–2128.
55 V. De Alencar Muniz Gonzaga, B. A. Chrisostomo, A. L. Poli and C. C. Schmitt, *Mater. Res.*, 2018, **21**(4), DOI: **10.1590/1980-5373-MR-2017-1024**.
56 T. M. Ho, A. Razzaghi, A. Ramachandran and K. S. Mikkonen, *Adv. Colloid Interface Sci.*, 2022, **299**, 102541.
57 C. J. M. Henríquez, W/O Emulsions: Formulation, Characterization and Destabilization, Dr thesis, 2009, **https://core.ac.uk/download/pdf/33428703.pdf**.